



Article

An Efficient and Accurate Approach to Electrical Boundary Layer Nanofluid Flow Simulation: A Use of Artificial Intelligence

Amani S. Baazeem ^{1,*}, Muhammad Shoaib Arif ^{2,3,*}  and Kamaleldin Abodayeh ³ 

¹ Department of Mathematics and Statistics, College of Science, Imam Mohammad Ibn Saud Islamic University (IMSIU), P.O. Box 90950, Riyadh 11623, Saudi Arabia

² Department of Mathematics, Air University, PAF Complex E-9, Islamabad 44000, Pakistan

³ Department of Mathematics and Sciences, College of Humanities and Sciences, Prince Sultan University, Riyadh 11586, Saudi Arabia

* Correspondence: asbaazeem@imamu.edu.sa (A.S.B.); marif@psu.edu.sa (M.S.A.)

Abstract: Engineering and technological research groups are becoming interested in neural network techniques to improve productivity, business strategies, and societal development. In this paper, an explicit numerical scheme is given for both linear and nonlinear differential equations. The scheme is correct to second order. Additionally, the scheme's consistency and stability are guaranteed. Backpropagation of Levenberg–Marquardt, the effect of including an induced magnetic field in a mathematical model for electrical boundary layer nanofluid flow on a flat plate, is quantitatively investigated using artificial neural networks. Later, the model is reduced into a set of boundary value problems, which are then resolved using the suggested scheme and a shooting strategy. The outcomes are also contrasted with earlier studies and the MATLAB solver bvp4c for validation purposes. In addition, neural networking is also employed for mapping input to outputs for velocity, temperature, and concentration profiles. These results prove that artificial neural networks can make precise forecasts and optimizations. Using a neural network to optimize the fluid flow in an electrical boundary layer while subjected to an induced magnetic field is a promising application of the suggested computational scheme. Fluid dynamics benefits greatly from combining numerical methods and artificial neural networks, which could lead to new developments in various fields. Results from this study may aid in optimizing fluid systems, leading to greater productivity and effectiveness in numerous technical fields.

Keywords: explicit scheme; stability; consistency; boundary layer flow; neural network



Citation: Baazeem, A.S.; Arif, M.S.; Abodayeh, K. An Efficient and Accurate Approach to Electrical Boundary Layer Nanofluid Flow Simulation: A Use of Artificial Intelligence. *Processes* **2023**, *11*, 2736. <https://doi.org/10.3390/pr11092736>

Academic Editors: Mohamed F. El-Amin, Osama Eljamal and Haiping Zhu

Received: 16 August 2023

Revised: 31 August 2023

Accepted: 9 September 2023

Published: 13 September 2023



Copyright: © 2023 by the authors. Licensee MDPI, Basel, Switzerland. This article is an open access article distributed under the terms and conditions of the Creative Commons Attribution (CC BY) license (<https://creativecommons.org/licenses/by/4.0/>).

1. Introduction

Fluid dynamics and the phenomena they produce have long piqued the interest of scientists and engineers. Several fields, such as the aerospace, automotive, and energy industries, rely heavily on fluid dynamics and flow optimization advances. Many mathematical models and computer systems have been developed for simulating and analyzing fluid flow. These models have been shown to predict how fluids will act in various situations accurately.

There has been a significant increase in research into how electromagnetic fields can affect fluid motion. Fluids' reactions to electric or magnetic fields have shown promise for improving flow regulation and thermal conductivity. The thin fluid layer next to a solid surface in the presence of an induced magnetic field is particularly important and is known as the electrical boundary layer. Flow properties like velocity profiles, shear stress distribution, and heat transfer rates are all heavily influenced by the electrical boundary layer.

This work introduces a unique computational scheme and neural network approach to studying fluid flow in electrical boundary layers in an induced magnetic field. With the proposed approach, we want to shed light on the complex dynamics between the boundary

layer's magnetic field and its fluid flow. Traditional analytical methods have limitations, but by utilizing the potential of computational modelling and artificial neural networks, we may overcome these obstacles and make more precise and efficient forecasts. Our computational framework uses numerical techniques like finite volumes to discretize the governing equations of fluid dynamics and electromagnetic fields. The Navier–Stokes and Maxwell's equations describe fluid and electromagnetic fields, respectively. By iteratively solving these linked equations, we may simulate the fluid's behavior within the electrical boundary layer and examine its characteristics under various magnetic field configurations. We propose adding neural networks to the modelling framework to improve our computational scheme's precision and speed. Neural networks have proven to be quite effective at identifying intricate relationships and patterns in data. This computational simulation data can be used to train a neural network to anticipate the electrical boundary layer's behavior for different values of input parameters, including magnetic field intensity, fluid characteristics, and surface geometry. This neural network-based method can drastically reduce the time needed to perform complex optimization and parametric study tasks.

Geophysics, magnetohydrodynamic (MHD) natural convection flow, heat exchangers, astrophysics, and electronics are just a few of the many fields that can benefit from taking magnetic fields into account during electrically conducted fluid flow. Plasma theory, as well as MHD coolants and generators, are examples of physical phenomena in which a magnetic field governs the flow of fluid. Some scholars have demonstrated interest in the many scientific and technical phenomena of induced magnetic fields. However, none of these studies have addressed the topic of how a generated magnetic field affects the flow of the boundary layer. An induced magnetic field has obvious uses in the plasma field as well. Among other things, the created magnetic field can be used to examine solar activity, cosmic rays, and subsurface water flow.

The effects of induced magnetic fields on ferrofluid flows on a flat plate are considered in [1]. The flow was brought about by the sudden shock of the plate, which was only partially finite. To simulate the flow caused by the induced magnetic field (IMF), the Navier–Stokes equation and a set of heat equations were combined. Before being transformed into ordinary differential equations (ODEs), the governing equations are typically represented as partial differential equations (PDEs) in the majority of the literature [2–4]. In most cases, researchers have only considered the effects on fluid flow in two dimensions [5–7]. The impact of various forces on boundary layer flows has been studied using two distinct approaches in the extant literature [8,9]. Various nanoparticles of varying kinds are sometimes added to the base fluid to improve heat transfer. The Buongiorno nanofluid model [10–12] provides a set of partial differential equations for nanofluids subject to the influence of heat and mass transfers and is another mathematical model for this class of fluids. Some authors investigate the Buongiorno model to simulate flows when the mass transfer equation is included in a system of equations. Oldroyd 4-constant nanofluid has been used to experiment with the induced magnetic flux [13]. Using a small finite Reynolds number has reduced the complexity of solving nonlinear partial differential equations. The differential equations under consideration have been solved exactly. The magnetic force function grew with both the magnetic Reynolds number and the electric field strength. Convective Casson fluid's response to the exponential heat source and an induced magnetic field is studied in [14].

In many sectors, including producing PVC pipes, wire drawing, metal casting, hot rolling, etc., boundary layer flow on a stretching sheet represents a significant fluid dynamics challenge. In [15,16], Sakidas presents his early research on the special characteristics of boundary layer flow over a stretched surface moving at a constant speed. Crane [17] analyzed the stretch surface at various speeds. Citation: Tsou et al. [18]. The most intriguing nanofluidic models can be found in [19–21], while some recent computational fluid dynamics applications addressing boundary layer flow can be seen in [22–24]. The role of the heat source and sink is critical in the boundary layer flow problem because cooling is required. The heat source and sink boundary layer flow problem on a stretching sheet was researched

by Cortell [25]. Dessie and Kishan [26] investigated how heat transmission in a permeable medium with varying viscosity might affect a stretched surface with a heat source and a heat sink. There are similarities between the research of the Abel group and similar studies conducted by other academics [27]. Aerospace engineering, specifically the design and analysis of re-entry vehicles like spacecraft or space capsules, is a fascinating real-world application demonstrating our work's importance. An electrically conductive boundary layer forms around the vehicle as it undergoes the high temperatures and pressures of re-entry into a planet's atmosphere. Due to the relative speed of the conducting vehicle and the ionized gases, magnetic fields are induced in this boundary layer. During re-entry, the heat transfer, aerodynamic forces, and overall vehicle behavior can all be drastically altered by these produced magnetic fields. We contribute significantly to fluid dynamics, electromagnetics, and heat transport by including the effects of induced magnetic fields in our numerical framework and employing neural networks to improve the accuracy of predictions. As a result, this information can be useful to aerospace engineers as they work to perfect the performance, safety, and thermal protection of re-entry vehicles.

Due to magnetic field intensities and fluid conditions, the Hall effect may not be justified in our investigation of induced magnetic fields in electrical boundary layer flows. The main focus is on understanding the interaction between the induced magnetic field and the fluid flow without considering ancillary effects that may not be relevant. The studies mentioned [28–30] examine instances where ion slip and Hall effects play a significant role under specific circumstances. In contrast, our study concentrates on the electrical boundary layer flow with generated magnetic fields, enabling us to simplify the model by excluding these effects. The decision to disregard these effects is supported by the comparatively moderate flow velocities, magnetic field strengths, and ion densities in the situations under consideration.

The authors investigate the radiative unsteady magnetohydrodynamic (MHD) flow of an incompressible viscous electrically conducting non-Newtonian Casson hybrid nanofluid over an infinite exponentially accelerated vertical moving porous surface, considering the influence of slip velocity in a rotating frame [31]. The primary objective of this study [32] is to investigate the phenomenon of coupled heat and mass transfer by natural convection. Specifically, the focus is on a fluid flow with micropolar characteristics that exhibits viscosity and generates or absorbs heat. The flow occurs in the vicinity of a vertically oriented, permeable surface that is in continuous motion. Additionally, the study considers the influence of a first-order chemical reaction. The issue of combined heat and mass transfer through natural convection from a semi-infinite inclined flat plate, considering the influence of an external magnetic field and internal heat generation or absorption effects, is presented in reference [33].

The incorporation of nanoparticles into a base fluid has been observed to induce substantial modifications in fluid behavior, owing to the distinctive features exhibited by nanoparticles at the nanoscale. Researchers have investigated methods to improve heat transfer rates, fluid conductivity, and other fluid properties by utilizing the capabilities of nanoparticles [34,35]. Incorporating nanoparticles into a fluid matrix gives rise to a composite material called a nanofluid. This composite material demonstrates improved thermal and electrical characteristics compared to the original fluid without nanoparticles. Nanoparticles have the potential to enhance heat conduction, optimize convective heat transfer, and modify flow characteristics, hence positioning nanofluids as viable contenders for a range of engineering applications. Heat exchangers play a crucial role in industrial processes, making a substantial contribution to the system's overall energy. The fouling process, the primary factor influencing heat exchanger performance, was thoroughly examined in a study conducted by [36]. Various fouling processes and models were dynamically simulated in this research.

An investigation into the traditional Blasius equation, which serves as the governing equation for the boundary layer problem, is carried out with the help of a numerical approach. The creation of the RCW (Rahmanzadeh–Cai–White) approach [37] is the

foundation for this algorithm and an investigation into how the Lorentz force and bleeding combine to affect the hydrothermal behaviors of magnetohydrodynamic (MHD) nanofluid flow and the formation of entropy in a trapezoidal recess. This trapezoidal recess is formed by incorporating two sloping steps into an otherwise horizontal channel. Because a magnetic field was present in the flow domain, the Lorentz force could manifest itself [38].

Artificial neural networks (ANNs) are particularly helpful among the many artificial intelligence (AI) techniques. ANNs have been applied in various fields because of their adaptability to nonlinear phenomena and capacity to model them. ANNs can learn and change based on their given data, making them useful in many fields. Artificial neural networks are useful in many areas, including system identification, sequence recognition, process control, sensor data analysis, natural resource management, quantum chemistry, medical diagnosis, financial analysis, visualization, machine translation, and e-mail spam filtering. Machine learning algorithms like artificial neural networks can be used to model intricate correlations in data. Because of this, they are suitable for various uses, including those mentioned above. Hence, the backpropagation stochastic numerical approach is more reliable. Backpropagation is a supervised learning method that uses gradient descent to lower the error curve's slope and minimize error.

Paul Werbos invented the backpropagation technique in 1974, and Rumelhart and Parker later brought it back to life. A common learning method for feed-forward multilayer neural networks is backpropagation. A unique convergent stability method for artificial neural networks called Levenberg–Marquardt (LM) backpropagation offers numerical answers to various fluid flow problems. Recent studies have used Levenberg–Marquardt backpropagation artificial neural networks (LBM-BN) on Newtonian and non-Newtonian hydraulic systems. Using an ANN model trained with the Levenberg–Marquardt method, Khalil et al. [39] provide a numerical solution for the non-Newtonian flow field. Zhao et al. [40] used the LBM-BN approach to identify the flaws in reinforced concrete beams. ANN-based LM was used by Nguyen et al. [41] to ensure more precise robot positioning. In order to forecast the outflow from a sharp-crested weir, Ali et al. [42] combined an artificial neural network strategy with an LM-based training method. According to Ye and Kim [43], their study focuses on the application of an optimized backpropagation neural network and the Levenberg–Marquardt backpropagation neural network to predict electricity usage in a building. The case study specifically examines a shopping mall located in China. The authors analyzed the thermally radiative and chemically reactive stagnation point flow of a non-Newtonian fluid with temperature-dependent thermal conductivity using the Levenberg–Marquardt training technique [44].

For the purpose of solving mathematical models of various processes, numerical approaches are crucial. The physical behavior of any system cannot be simply predicted from its mathematical model, which is expressed in the form of differential equations. Different approaches do, however, exist to resolve various kinds of differential equations. This contribution makes explicit use of a two-stage numerical approach. The Taylor extension of the forward Euler scheme is the first phase. As a result, when first-order differential equations are solved, an additional derivative of the dependent variable is needed. A shooting method is used to implement the suggested scheme because the considered problems are second- and third-order boundary value problems. Thus, the model's solution is discovered in this way.

This paper makes two main contributions. We introduce a robust computational scheme for studying fluid flow in an electrical boundary layer in the presence of an induced magnetic field. Using a combination of neural networks and numerical approaches, the scheme can make precise predictions and run rapid simulations. Second, we show that our method works by comparing it to analytical and numerical solutions already developed. These examples demonstrate the precision, efficiency, and adaptability of our system.

2. Proposed Numerical Scheme

Suppose we have a differential equation of the type for constructing a numerical scheme for a differential equation.

$$u' = \lambda f(u) \quad (1)$$

where λ is a constant.

The initial phase of the scheme outlined in Equation (1) can be formulated as:

$$\bar{u}_i = u_{i-1} + hu'_{i-1} + h^2u''_{i-1} \quad (2)$$

where h is the step size.

The second stage of the scheme is given as follows:

$$u_i = \frac{1}{2}(u_{i-1} + \bar{u}_i) + h\{au'_{i-1} + b\bar{u}'_i\} \quad (3)$$

where a and b are unknown, to be determined later.

The Taylor series expansion for u_{i-1} and u'_{i-1} is given as:

$$u_{i-1} = u_i - hu'_i + \frac{h^2}{2}u''_i + O(h^3) \quad (4)$$

$$u'_{i-1} = u'_i - hu''_i + O(h^2) \quad (5)$$

Substituting Equations (4) and (5) into Equation (3) we obtain

$$u_i = \frac{1}{2}\left(u_i - hu'_i + \frac{h^2}{2}u''_i + \bar{u}_i\right) + h\{au'_i - ah u''_i + b\bar{u}'_i\} \quad (6)$$

By using Equation (2) in Equation (6) it yields

$$u_i = \frac{1}{2}\left(u_i - hu'_i + \frac{h^2}{2}u''_i + u_{i-1} + hu'_{i-1} + h^2u''_{i-1}\right) + h\{au'_i - ah u''_i + bu'_i + bh u''_i\} \quad (7)$$

Expanding u_{i-1} , u'_{i-1} and u''_{i-1} using Taylor series expansion

$$u_i = u_i - \frac{1}{2}hu'_i + \frac{h^2}{2}u''_i + h\{au'_i - ah u''_i + bu'_i\} \quad (8)$$

By comparing coefficients of hu'_i and $h^2u''_i$ on both sides of Equation (8), it gives

$$0 = -\frac{1}{2} + a + b \quad (9)$$

$$0 = \frac{1}{2} - a \quad (10)$$

By solving (9) and (10), it yields

$$a = \frac{1}{2}, b = 0 \quad (11)$$

Therefore, the second stage of the scheme is given as

$$u_i = \frac{1}{2}(u_{i-1} + \bar{u}_i) + \frac{h}{2}u'_{i-1} \quad (12)$$

3. Stability Analysis

Consider the linear differential equation of the form to determine the stability region of the proposed scheme.

$$v' = \mu v \quad (13)$$

Using the first stage of the proposed scheme for Equation (13) it gives:

$$\bar{v}_i = v_{i-1} + h\mu v_{i-1} + h^2\mu^2 v_{i-1} = (1 + z + z^2)v_{i-1} \quad (14)$$

where $z = h\mu$.

The second stage of the proposed scheme for Equation (14) yields:

$$\begin{aligned}v_i &= \frac{1}{2}(v_{i-1} + \bar{v}_i) + \frac{h}{2}\mu v_{i-1} \\v_i &= \frac{1}{2}(2 + z + z^2)v_{i-1} + \frac{z}{2}v_{i-1} \\v_i &= \frac{1}{2}(2 + 2z + z^2)v_{i-1}\end{aligned}\quad (15)$$

Thus the stability region is given as

$$\left| \frac{1}{2}(2 + 2z + z^2) \right| \leq 1, \quad z \in \mathbb{C} \quad (16)$$

4. Consistency of the Proposed Scheme

For checking the consistency of the proposed scheme for Equation (13), Equation (15) is re-written as:

$$v_i = \frac{1}{2}(2 + 2h\mu + h^2\mu^2)v_{i-1} \quad (17)$$

Expanding v_{i-1} using Taylor series expansion yields

$$\begin{aligned}v_i &= \frac{1}{2}(2 + 2h\mu + h^2\mu^2) \left(v_i - hv'_i + \frac{h^2}{2}v''_i \right) \\v_i &= v_i - hv'_i + \frac{h^2}{2}v''_i + h\mu v_i - h^2\mu v'_i + \frac{h^3}{2}\mu v''_i + h^2\mu^2 v_i - h^3\mu^2 v'_i + \frac{h^4}{2}\mu^2 v''_i + O(h^5)\end{aligned}\quad (18)$$

Dividing both sides by h and simplifying gives

$$v'_i = \mu v_i + O(h) \quad (19)$$

Applying *limit* $h \rightarrow 0$ to Equation (19)

$$v'_i = \mu v_i \quad (20)$$

Which is the original differential Equation (13) evaluated at grid point i .

5. Problem Formulation

Think about a steady, incompressible, laminar, two-dimensional fluid flow across the sheet. The sheet moves toward the positive x -axis, and the y -axis is taken perpendicular to the sheet. A strong magnetic field is made use of perpendicular to the sheet. The impact of the IMF is considered, with the magnetic Reynolds number assumed to be high. Suppose the value of H_y at the sheet is zero, i.e., $H_y = 0$. Let $U_w = ax$ where a is the constant is the velocity of the sheet. Transverse magnetic field and uniform electric field are applied to an electrically conductive fluid. It is assumed that the magnetic field follows Ohm's law and is weaker than the electric field. The geometry of this flow phenomenon over the stretching sheet can be seen in Figure 1. The governing equations are represented by adhering to the boundary layer theory's premise [45].

$$\frac{\partial u}{\partial x} + \frac{\partial v}{\partial y} = 0 \quad (21)$$

$$\frac{\partial H_x}{\partial x} + \frac{\partial H_y}{\partial y} = 0 \quad (22)$$

$$u \frac{\partial u}{\partial x} + v \frac{\partial u}{\partial y} - \frac{\mu_e}{4\pi\rho} \left(H_x \frac{\partial H_x}{\partial x} + H_y \frac{\partial H_x}{\partial y} \right) = \nu \frac{\partial^2 u}{\partial y^2} - \frac{\mu_e H_e}{4\pi\rho} \frac{\partial H_x}{\partial x} + \frac{\sigma}{\rho} (E_\infty B_\infty - B_\infty^2 u) \quad (23)$$

$$u \frac{\partial H_x}{\partial x} + v \frac{\partial H_x}{\partial y} - \left(H_x \frac{\partial u}{\partial x} + H_y \frac{\partial u}{\partial y} \right) = \alpha_1^2 \frac{\partial^2 u}{\partial y^2} \quad (24)$$

$$u \frac{\partial T}{\partial x} + v \frac{\partial T}{\partial y} = \alpha \frac{\partial^2 T}{\partial y^2} + \frac{\nu}{c_p} \left(\frac{\partial u}{\partial y} \right)^2 + \tau \left(D_B \frac{\partial C}{\partial y} \frac{\partial T}{\partial y} + \frac{D_T}{T_\infty} \left(\frac{\partial T}{\partial y} \right)^2 \right) + \frac{\sigma}{\rho c_p} (u B_o - E_o)^2 \quad (25)$$

$$u \frac{\partial C}{\partial x} + v \frac{\partial C}{\partial y} = D_B \frac{\partial^2 C}{\partial y^2} + \frac{D_T}{T_\infty} \frac{\partial^2 T}{\partial y^2} - k_1 (C - C_\infty) \quad (26)$$

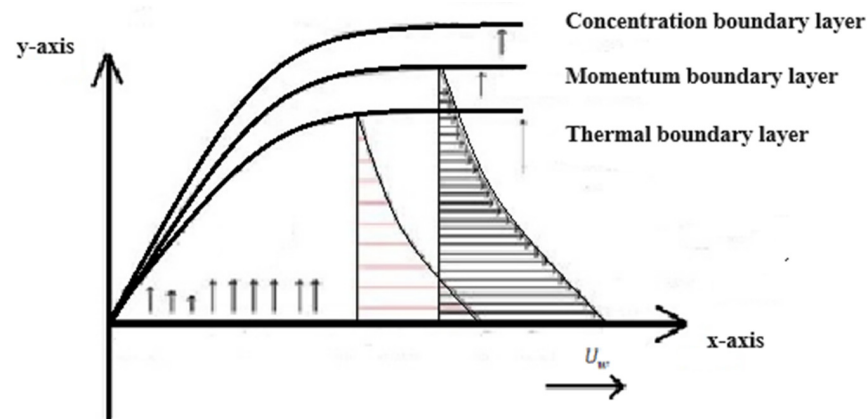


Figure 1. Geometry of the problem.

Subject to the boundary conditions

$$\left. \begin{aligned} u = U_w, v = 0, H_x = H_o \left(\frac{x}{l} \right), H_y = 0, T = T_w, C = C_w \text{ when } y = 0 \\ u \rightarrow 0, H_x \rightarrow 0, T \rightarrow T_\infty, C \rightarrow C_\infty, \text{ when } y \rightarrow \infty \end{aligned} \right\} \quad (27)$$

Under the transformations

$$u = axf', v = -\sqrt{av}f, \eta = \sqrt{\frac{a}{v}}y, H_x = H_o \left(\frac{x}{l} \right) g'(\eta),$$

$$H_y = -\sqrt{\frac{v}{a}}H_o \left(\frac{1}{l} \right) g(\eta), \theta = \frac{T - T_\infty}{T_w - T_\infty}, \phi = \frac{C - C_\infty}{C_w - C_\infty}$$

Equations (21)–(27) can be expressed as:

$$f'^2 - ff'' = f'' - \beta(g'^2 + gg'') + M(E_1 - f') \quad (28)$$

$$\delta g''' = -fg'' + f''g \quad (29)$$

$$-f\theta' = \frac{1}{Pr}\theta'' + E_c f'^2 + ME_c(f' - E_1)^2 + N_b\theta'\phi' + N_t\theta'^2 \quad (30)$$

$$-f\phi' = \frac{1}{Sc}\phi'' + \frac{N_t}{N_b}\theta'' - \gamma\phi \quad (31)$$

subject to the boundary conditions

$$\left. \begin{aligned} f = 0, f' = 1, g = 0, g' = 1, \theta = 1, \phi = 1 \text{ at } \eta = 0 \\ f' \rightarrow 0, g' \rightarrow 0, \theta \rightarrow 0, \phi \rightarrow 0 \text{ when } \eta \rightarrow \infty \end{aligned} \right\} \quad (32)$$

where

$$\beta = \frac{\mu_o H_o^2}{4\pi\rho a^2 l^2}, M = \frac{\sigma B_o^2}{a\rho}, \delta = \frac{\alpha_1}{v}, E_c = \frac{U_w^2}{c_p(T_w - T_\infty)}, N_b = \frac{\tau D_B(C_w - C_\infty)}{v},$$

$$N_t = \frac{\tau D_T(T_w - T_\infty)}{vT_\infty}, Pr = \frac{\nu}{\alpha}, Sc = \frac{\nu}{D_B}, E_1 = \frac{E_o}{B_o U_w}, \gamma = \frac{k_1}{a}$$

The skin friction coefficients and local Nusselt and Sherwood numbers are given by

$$C_f = \frac{\tau_w}{\rho U_w^2}, N_{u_x} = \frac{xq_w}{k(T_w - T_\infty)}, S_{h_x} = \frac{xJ_w}{D_B(C_w - C_\infty)} \quad (33)$$

$$\text{where } \tau_w = -\mu \left. \frac{\partial u}{\partial y} \right|_{y=0}, q_w = -k \left. \frac{\partial T}{\partial y} \right|_{y=0}, J_w = -D_B \left. \frac{\partial C}{\partial y} \right|_{y=0}.$$

Under mentioned transformations, dimensionless skin friction coefficients and dimensionless local Nusselt and Sherwood numbers are expressed as:

$$R_{e_x}^{\frac{1}{2}} C_f = -f''(0) \quad (34)$$

$$R_{e_x}^{-\frac{1}{2}} N_{u_x} = -\theta'(0) \quad (35)$$

$$R_{e_x}^{-\frac{1}{2}} S_{h_x} = -\phi'(0) \quad (36)$$

6. Results and Discussion

The suggested strategy's second-order accuracy can be confirmed using Taylor series expansion. The utilization of the Gauss–Seidel iterative approach in the suggested strategy aligns well with the stability analysis that has been previously discussed. The stability of the scheme affects its capacity to converge. The scheme is conditionally stable, which leads to its conditional convergence. An additional iterative method called the Gauss–Seidel method is adopted to find the solutions to the proposed scheme. It is necessary to provide an initial estimate to initiate the solution procedure of the Gauss–Seidel iterative method. The proposed scheme's and the Gauss–Seidel iterative method's convergence of the solution are also dependent on stopping criteria written in MATLAB code. The ultimate solution will be found if the provided stopping requirements are met; otherwise, calculations will continue until the loop's final limit is reached. The solution's biggest norm over two iterations is the basis for this contribution's halting criterion. If the maximum value falls below the specified tolerance in the proximity of zero, the iterative process will terminate, and the relevant data will be employed for simulation purposes. The utilization of a shooting method is also employed in the resolution of second- and high-order boundary value issues because the suggested methodology exclusively addresses first-order differential equations. The proposed scheme and the MATLAB solver `fsolve` for solving equations form the basis of the shooting strategy for this contribution. Therefore, two sets of starting estimates are needed for the solution method shown in this contribution. The one for the Gauss–Seidel iterative approach is outlined earlier in this article, and the other is for the MATLAB solver `fsolve`.

The effect of magnetic and local electric factors on the velocity profile is depicted in Figure 2. By increasing local electric parameters and magnetic factors, velocity exhibits a dual characteristic. The impact of M and δ on f' and g' are depicted in Figure 3. The velocity profile decays by rising M while g' rises by enhancing δ . As the Lorentz force opposing the velocity profile increases, the velocity profile degrades. The impact of Eckert and Prandtl numbers on temperature profile θ is displayed in Figure 4. Eckert and Prandtl numbers are increased and decreased to create the temperature profile. Internal friction between fluid particles causes the temperature profile to climb as the Eckert number increases. Lower thermal conductivity due to declining thermal diffusivity as the Prandtl number rises is what causes the temperature profile to degrade. Temperature profiles θ as a function of thermophoresis and Brownian motion parameters are shown in Figure 5. By increasing thermophoresis and Brownian motion parameters, the temperature profile rises. The improvement in the thermophoresis force causes the temperature profile to rise due to increasing thermophoresis parameters. Cold particles travel toward the plate as a result of the force of thermophoresis, which draws hot fluid particles to their vicinity.

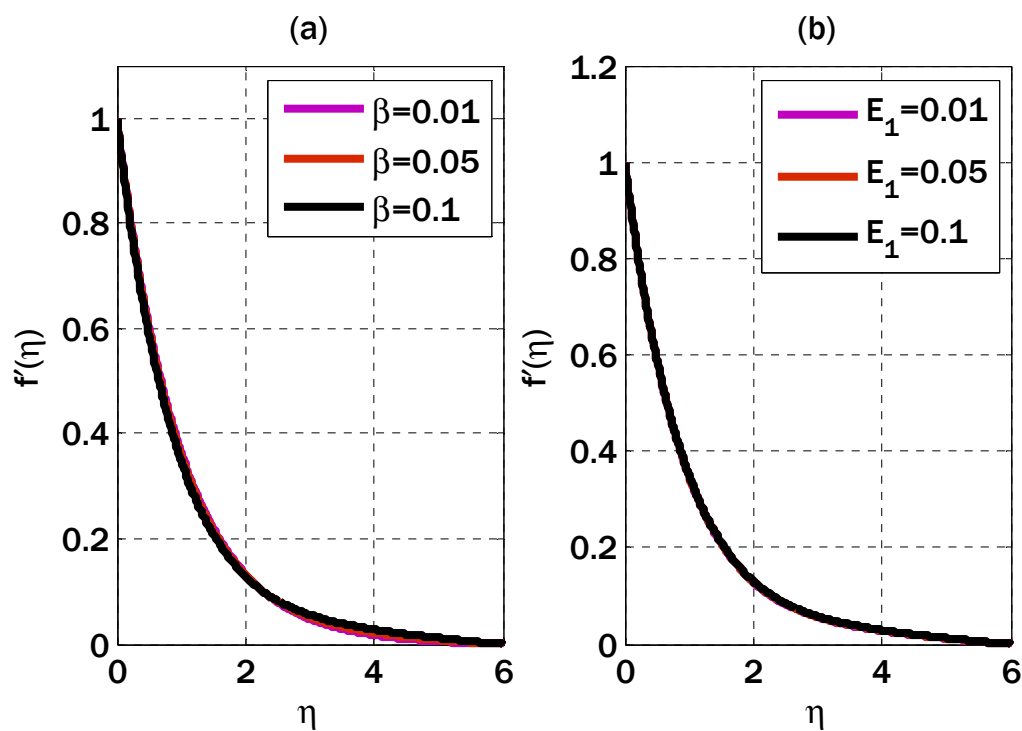


Figure 2. Impact of magnetic parameter β and local electric parameter on velocity profile using $M = 0.01, \delta = 3$. (a) $E_1 = 0.01$; (b) $\beta = 0.1$.

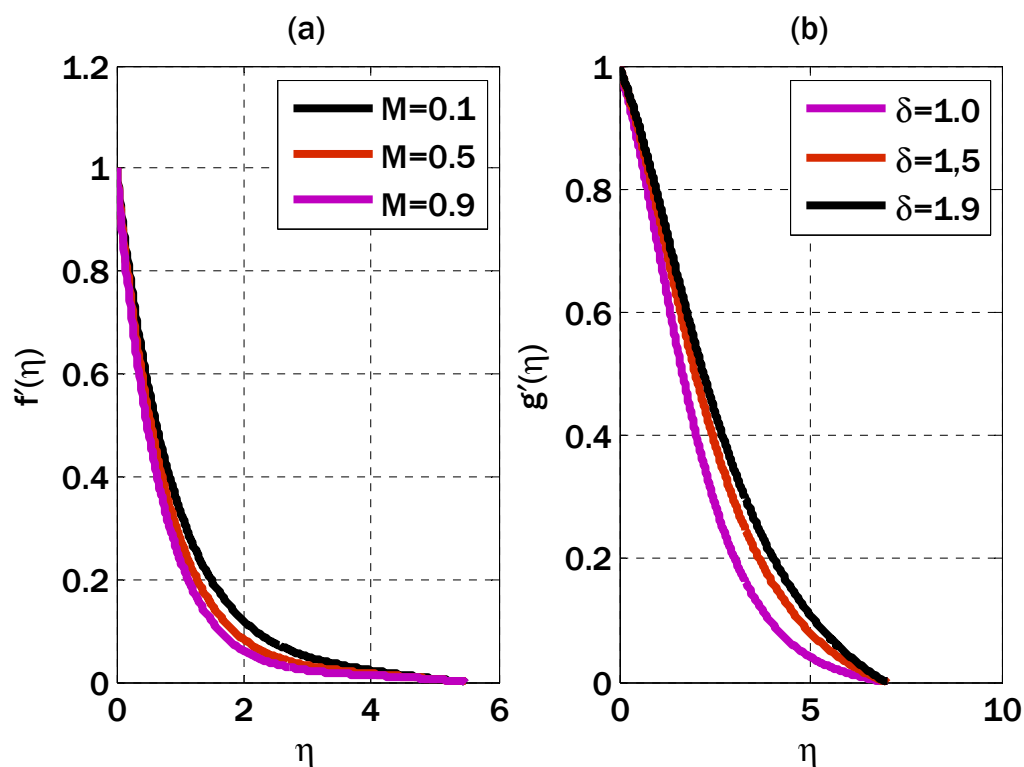


Figure 3. Impact of magnetic parameter M and reciprocal of magnetic Prandtl number on velocity profile using $E_1 = 0.01, \beta = 0.1$. (a) $\delta = 3$; (b) $M = 0.5$.

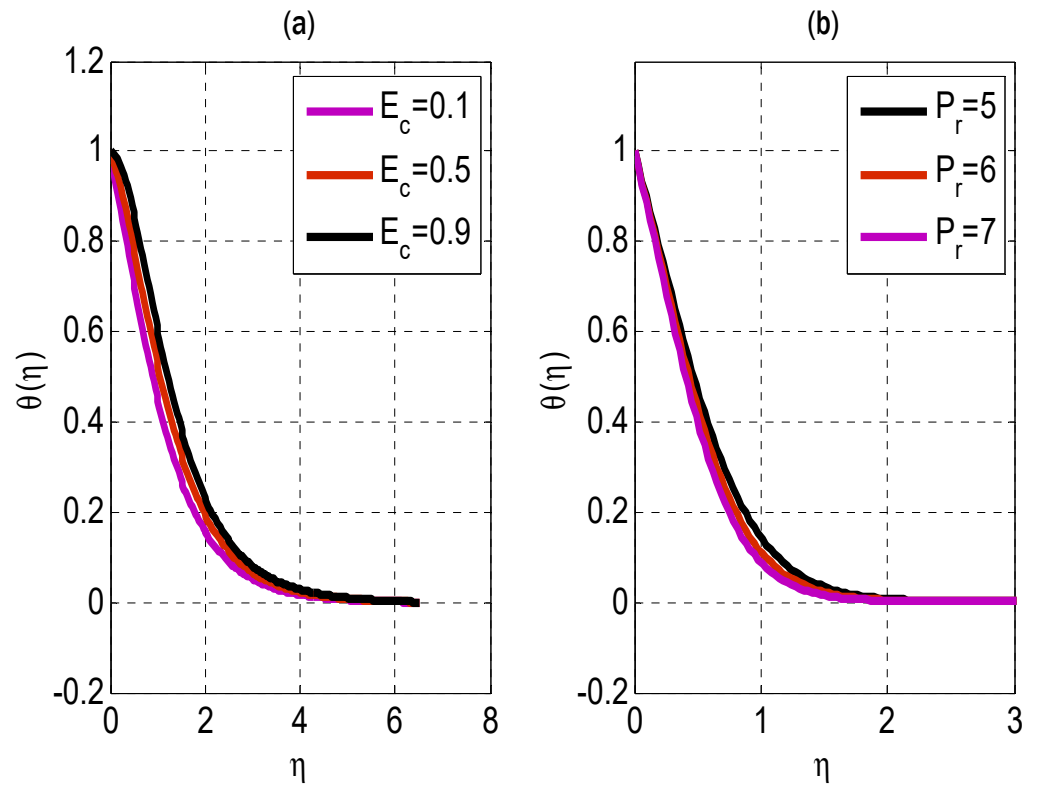


Figure 4. Impact of Eckert number and Prandtl number on temperature profile using $E_1 = 0.1, \beta = 0.1, M = 0.05, \delta = 1.4, N_t = 0.1, N_b = 0.1, S_c = 1.5, \gamma = 0.5$. (a) $P_r = 1.5$; (b) $E_c = 0.1$.

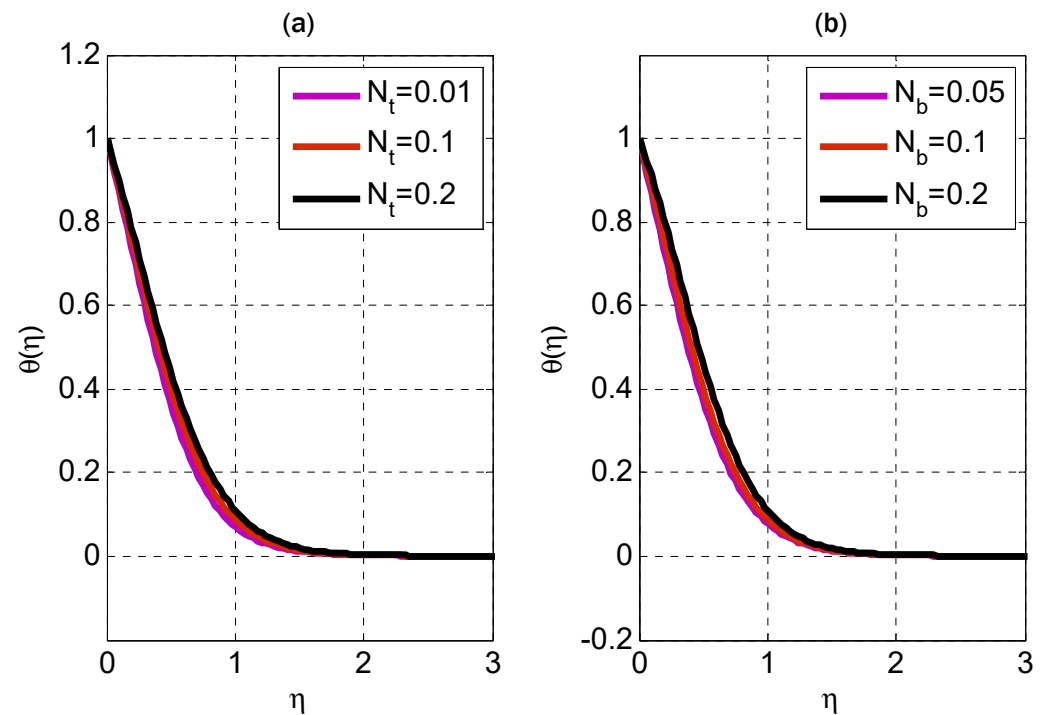


Figure 5. Impact of thermophoresis and Brownian motion parameters on temperature profile using $E_1 = 0.1, \beta = 0.1, M = 0.05, \delta = 1.4, E_c = 0.1, P_r = 7, S_c = 1.5, \gamma = 0.5$. (a) $N_b = 0.1$; (b) $N_t = 0.1$.

Additionally, the hotter particles are randomized in a different direction due to the development in the Brownian motion parameter spreads. The temperature profile rises as a result. Concentration profiles for varying Schmidt numbers and reaction rate parameters are shown in Figure 6. The quality of the concentration profile decreases as the Schmidt

number rises. As the Schmidt number increases, the concentration profile increases due to the loss in mass diffusivity.

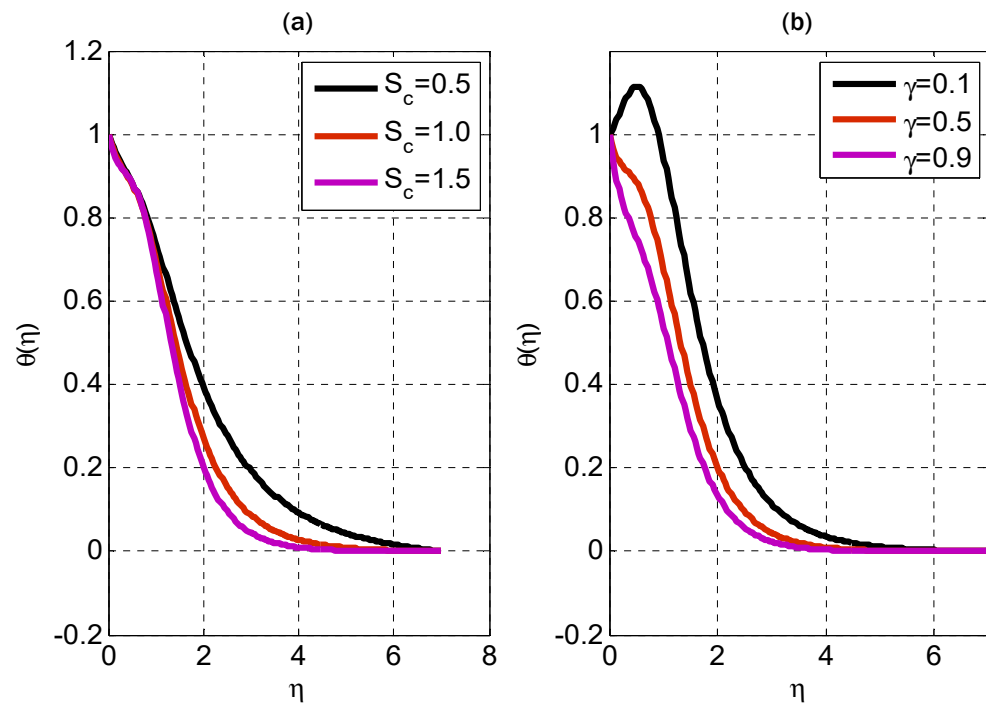


Figure 6. Impact of Schmidt number and reaction rate parameter on concentration profile using $E_1 = 0.1, \beta = 0.1, M = 0.05, \delta = 1.4, E_c = 0.1, Pr = 7, N_b = 0.1, N_t = 0.1$ (a) $\gamma = 0.5$ (b) $S_c = 1.5$.

As demonstrated in Table 1, the results from this contribution have been confirmed. The results will be the same if you use the MATLAB algorithm bvp4c. The bvp4c algorithm provides a high-order technique. The results are also contrasted with those of earlier research. Table 2 displays the numerical values of the skin friction coefficient as the magnetic parameter, local electric parameter, and the reciprocal of the magnetic parameter are varied. The skin friction coefficient changes depending on the local electric parameter, the magnetic parameter, and the inverse of the magnetic Prandtl number. Table 3 shows that the Eckert number, Prandtl number, and the thermophoresis parameter all affect the local Nusselt number.

Table 1. Comparison of the proposed scheme with past research for finding numerical values of $-f''(0)$ using $E_1 = \beta = 0, N(\text{no. of grid points}) = 500$.

M	Hayat et al. [46]	Yih [47]	Proposed	MATLAB bvp4c
0.0	1.000000	1.0000	1.0005	1.0002
0.5	1.224747	1.2247	1.2275	1.2247
1.0	1.414217	1.4142	1.4189	1.4142
1.5	1.581147	1.5811	1.5867	1.5811
2.0	1.732057	1.7321	1.7384	1.7321

Table 2. List of numerical values for skin friction coefficient using $M = 0.1$.

β	E_1	δ	$-f''(0)$
0.01	0.01	0.9	1.0523
0.1	0.01	0.9	1.0860
0.01	0.1	0.9	1.0404
0.01	0.01	1.5	1.0530

Table 3. List of numerical values for local Nusselt number using $\beta = 0.01, E_1 = 0.01, M = 0.1, \delta = 1.5, S_c = 1.5, \gamma = 0.9$.

N_t	N_b	E_c	P_r	$-\theta'(0)$
0.01	0.01	0.1	5	1.3159
0.02				1.3000
0.01	0.02			1.2855
	0.01	0.5		0.5491
		0.1	5.5	1.3821

On the other hand, raising the Eckert or Prandtl number causes the local Nusselt number to rise, while raising the thermophoresis or Brownian motion parameters decreases it. Table 4 demonstrates how thermophoresis, Brownian motion, the Schmidt number, and the dimensionless reaction rate influence the numerical values of local Sherwood numbers. When the Brownian motion parameter, the Schmidt number, and the thermophoresis parameter increase, the dimensionless response rate parameter falls.

Table 4. List of numerical values for local Sherwood number using $\beta = 0.01, E_1 = 0.01, M = 0.1, \delta = 1.5, P_r = 5, E_c = 0.1$.

N_t	N_b	S_c	γ	$-\phi'(0)$
0.01	0.02	1.5	0.9	0.9783
0.015				0.7723
0.01	0.025			1.0714
	0.02	1.9		1.0974
		1.5	1	1.0490

Using the Levenberg–Marquardt (LM) technique and computational scheme for fluid flow in an electrical boundary layer due to an induced magnetic field is a novel approach to this difficult problem. Finding an approximation to the solution of a system of nonlinear equations is possible with the help of the LM method, a powerful optimization tool. As a strong tool for solving partial differential equations, the finite element method (FEM) forms the basis of the computational architecture. The governing equations for fluid flow in an electrical boundary layer are solved using the LM method, which is then used to determine the best values for the relevant parameters. The fluid's temperature, the intensity of the magnetic field, and viscosity are all examples of such variables. The governing equations for the flow and temperature distribution are then solved using the computational scheme.

Some advantages of the LM method and computational methodology for fluid flow in electrical boundary layers subject to an induced magnetic field are as follows.

1. Finding an approximation to the solution of a system of nonlinear equations is possible with the help of the LM method, a powerful optimization tool. As a result, it can be used effectively to address the difficult equations describing fluid flow in an electrical boundary layer.
2. The finite element method (FEM), an effective method for solving partial differential equations, forms the basis of the computational process. This guarantees a correct and trustworthy solution to the equations.
3. The utilization of the LM approach and computational scheme enables the simulation of various situations encompassing diverse viscosities, magnetic field intensities, and temperatures. This characteristic renders it a valuable instrument for investigating the fluid dynamics of electrical boundary layer flow.

The study of artificial neural networks for the inputs and outputs of the model under consideration is also presented here. Three inputs represent the velocity, temperature, and concentration profiles. For these simulations, a two-layer feed-forward network is considered. For enough memory, the Levenberg–Marquardt backpropagation algorithm

trains the network; otherwise, scaled conjugate gradient backpropagation is utilized by nftool. A total of 70% of samples were used for training, 15% for validation, and 15% for testing. In addition, 10 was the number of hidden neurons that were considered. For the simulation of input and output of velocity, 891 iterations were consumed. One hundred fifty-eight iterations for the network training corresponding to the temperature profile were consumed. The algorithm consumed one hundred ninety-one iterations corresponding to the concentration profile. The most successful velocity, temperature, and concentration profile validation results are displayed in Figures 7–9, respectively. The error histograms for the training, validation, and test datasets are displayed in Figures 10–12. These error histograms also show zero error. The zero error is the minimum error achieved by the set of samples for training, validation, and testing. Figures 13–15 show the regression analysis. Figures 13–15 show how closely the output is related to the target.

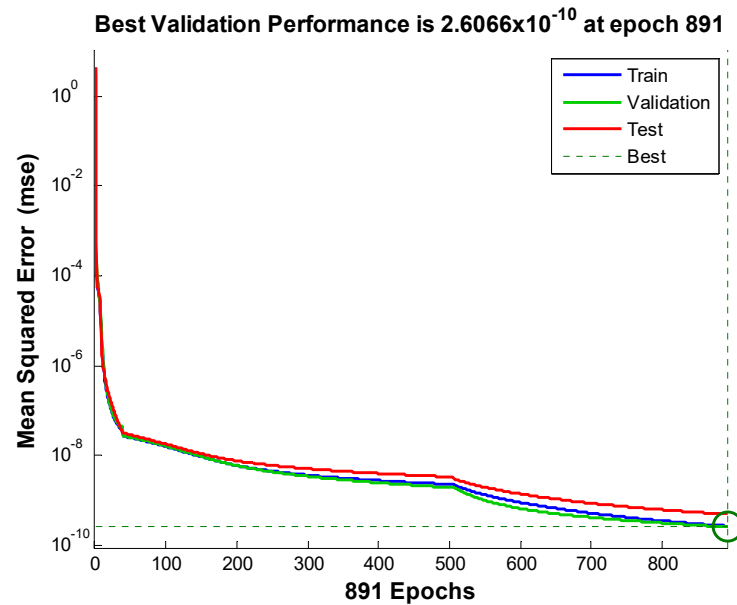


Figure 7. Performance plot for velocity model using. $E_1 = 0.01, \beta = 0.01, M = 0.1, \delta = 1.5, E_c = 0.1, P_r = 5, N_b = 0.02, N_t = 0.01, \gamma = 1, S_c = 1.5$.

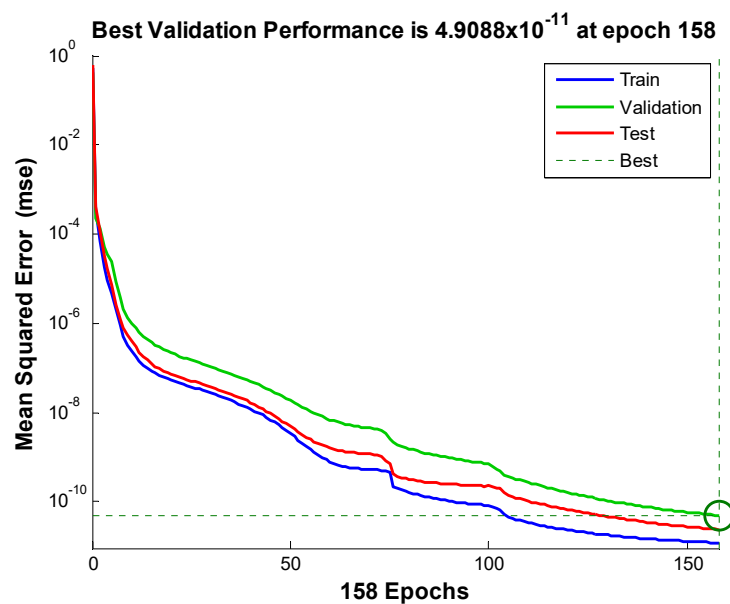


Figure 8. Performance plot for temperature model using $E_1 = 0.01, \beta = 0.01, M = 0.1, \delta = 1.5, E_c = 0.1, P_r = 5, N_b = 0.02, N_t = 0.01, \gamma = 1, S_c = 1.5$.

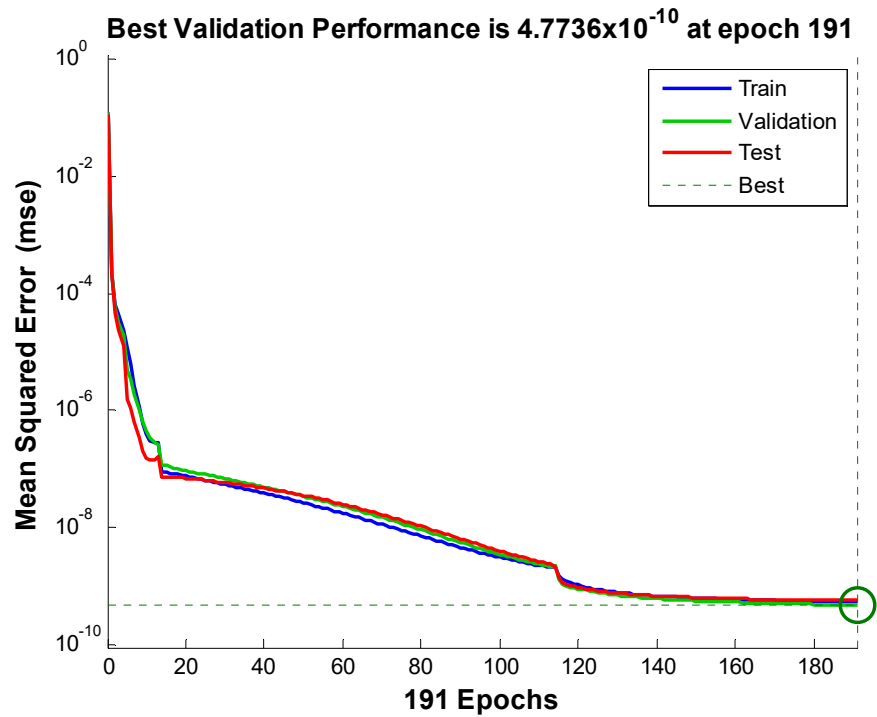


Figure 9. Performance plot for concentration model using $E_1 = 0.01, \beta = 0.01, M = 0.1, \delta = 1.5, E_c = 0.1, P_r = 5, N_b = 0.02, N_t = 0.01, \gamma = 1, S_c = 1.5$.

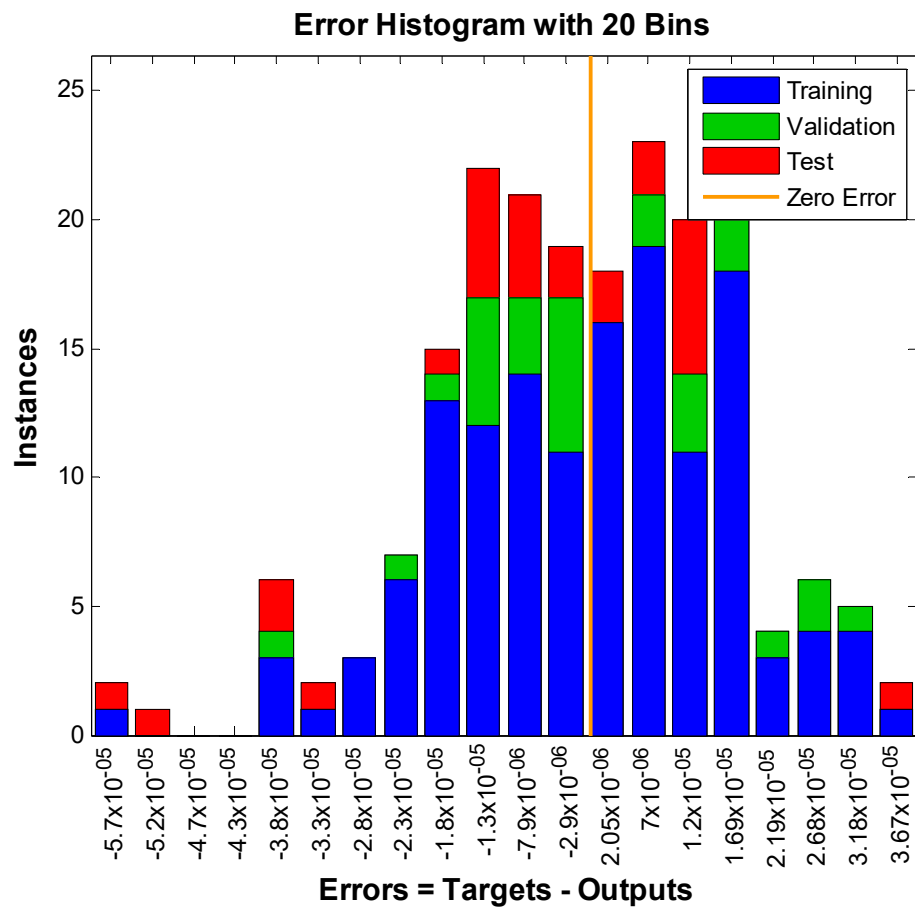


Figure 10. Error histogram for velocity model using $E_1 = 0.01, \beta = 0.01, M = 0.1, \delta = 1.5, E_c = 0.1, P_r = 5, N_b = 0.02, N_t = 0.01, \gamma = 1, S_c = 1.5$.

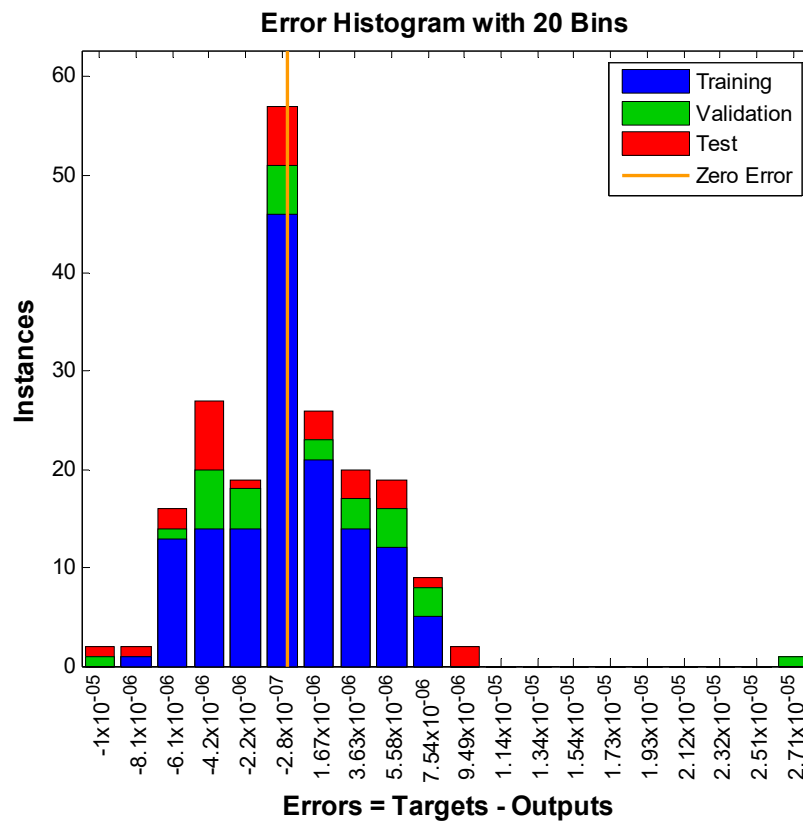


Figure 11. Error histogram for temperature model using $E_1 = 0.01, \beta = 0.01, M = 0.1, \delta = 1.5, E_c = 0.1, P_r = 5, N_b = 0.02, N_t = 0.01, \gamma = 1, S_c = 1.5$.

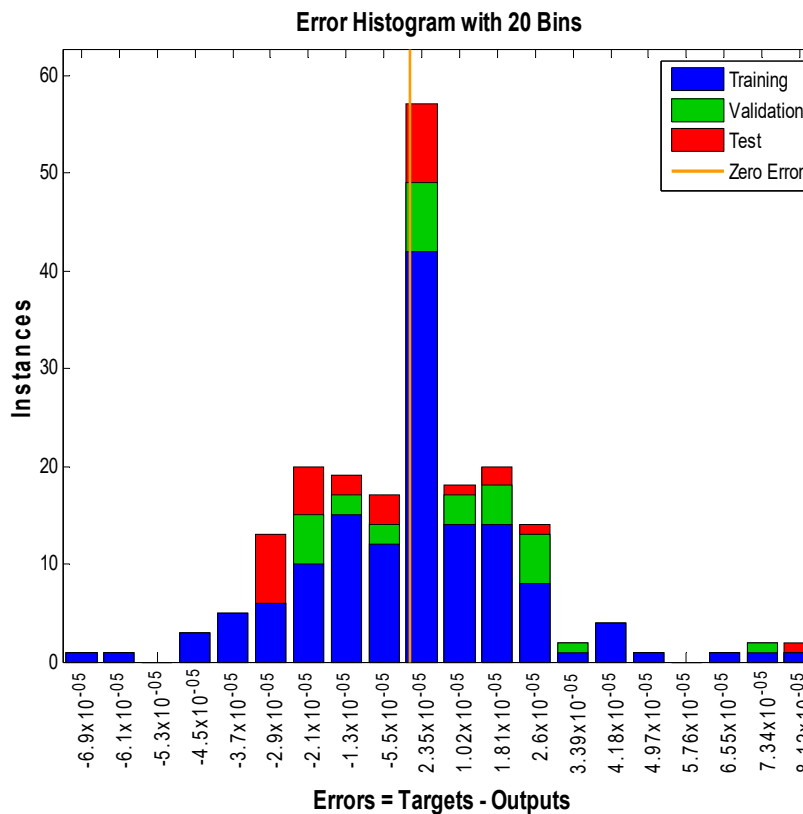


Figure 12. Error histogram for concentration model using $E_1 = 0.01, \beta = 0.01, M = 0.1, \delta = 1.5, E_c = 0.1, P_r = 5, N_b = 0.02, N_t = 0.01, \gamma = 1, S_c = 1.5$.

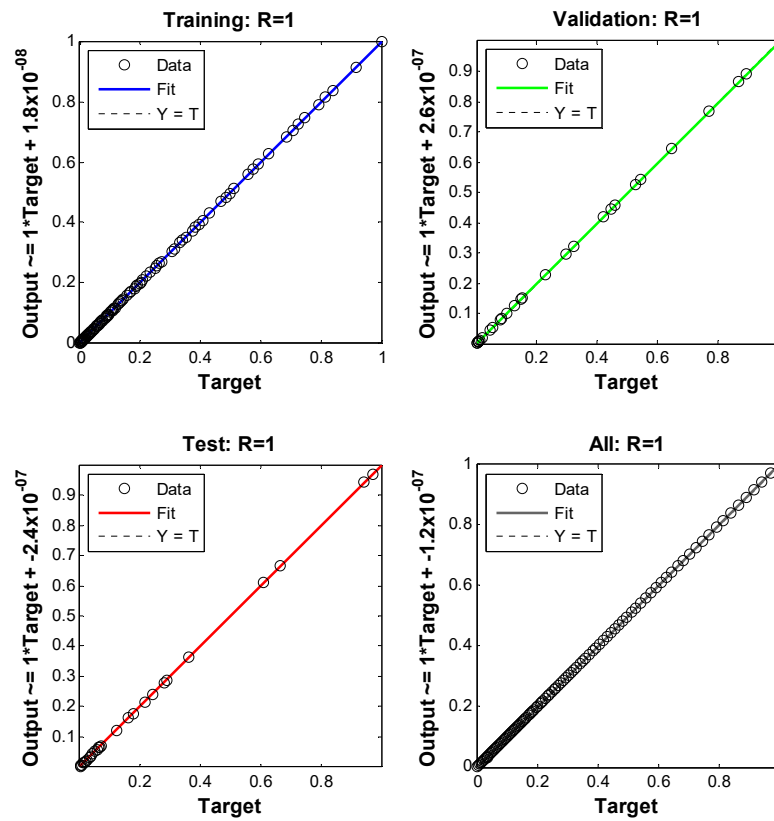


Figure 13. Regression plot for velocity model using $E_1 = 0.01, \beta = 0.01, M = 0.1, \delta = 1.5, E_c = 0.1, P_r = 5, N_b = 0.02, N_t = 0.01, \gamma = 1, S_c = 1.5$.

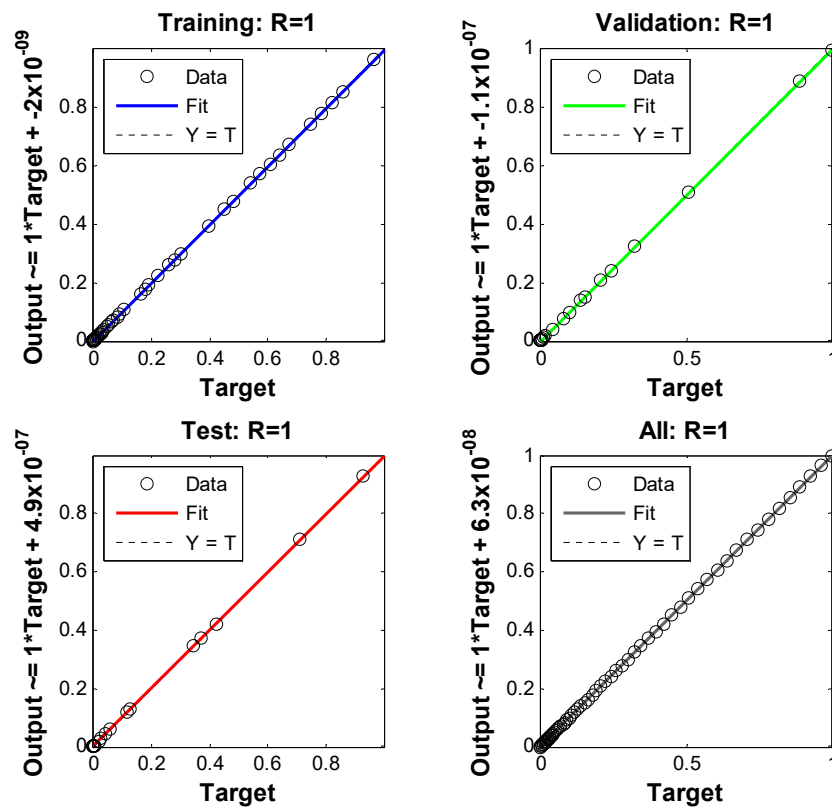


Figure 14. Regression plot for temperature model using $E_1 = 0.01, \beta = 0.01, M = 0.1, \delta = 1.5, E_c = 0.1, P_r = 5, N_b = 0.02, N_t = 0.01, \gamma = 1, S_c = 1.5$.

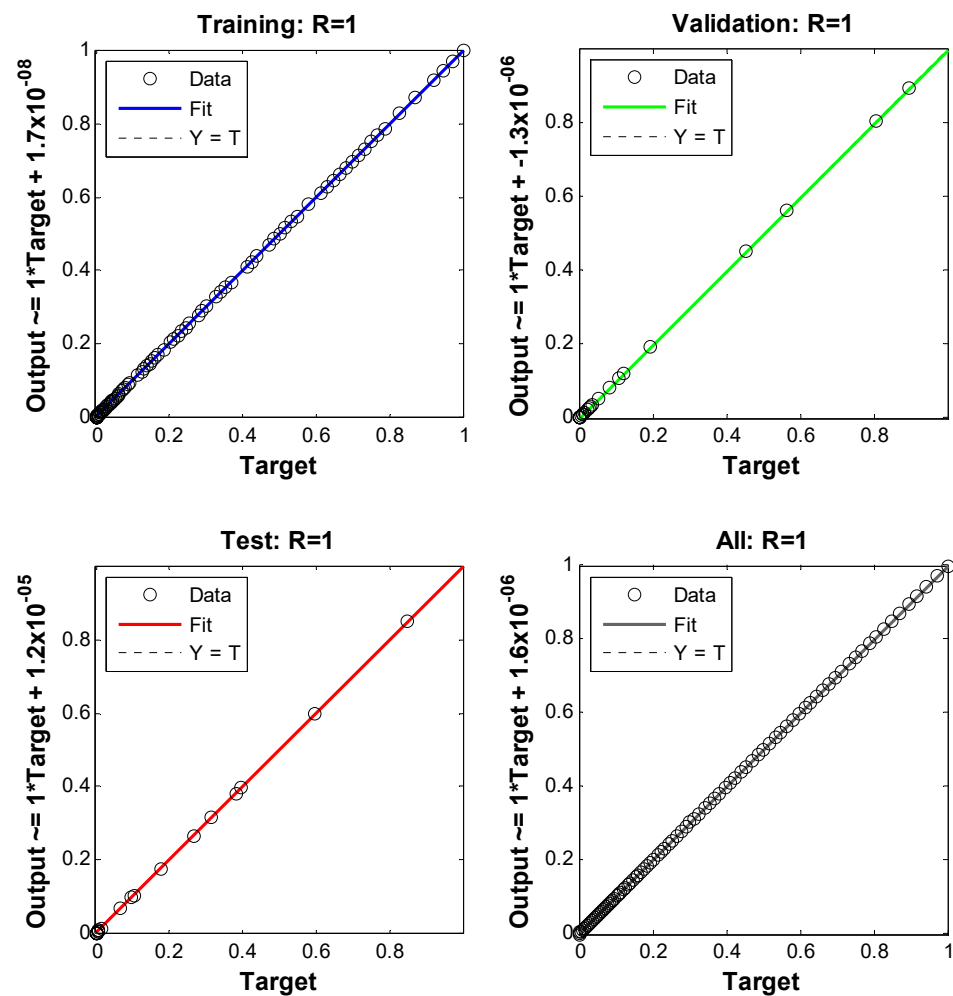


Figure 15. Regression plot for concentration model using $E_1 = 0.01$, $\beta = 0.01$, $M = 0.1$, $\delta = 1.5$, $E_c = 0.1$, $P_r = 5$, $N_b = 0.02$, $N_t = 0.01$, $\gamma = 1$, $S_c = 1.5$.

7. Conclusions

An explicit numerical scheme has been proposed and some of its analysis was provided when applied to the linear differential equation. Since the scheme can only be used for higher-order initial value problems or a system of first-order ODEs, a shooting approach is adopted for second- or third-order ODEs. The combined scheme has been applied to the dimensionless heat and mass transfer model of boundary layer flow under the induced magnetic field. Our findings have wider ramifications than just theoretical progress. The insights generated from our computational framework and neural network approach can aid in optimizing fluid systems in the real world. Better understanding and control of fluid flow properties can assist the aerospace, automotive, and energy industries. These systems potential for improvement in efficiency and performance has the potential to pave the way for significant technological and resource utilization advances. More advanced fluid phenomena and incorporating other physical elements can be considered by broadening the scope of our computational method in future studies. Using new neural network topologies and training techniques, our surrogate models can be more accurate and efficient. Our study paves the way for future advancement and innovation in fluid dynamics research and applications by providing a solid groundwork for further investigation and development of computational approaches for electrical boundary layer fluid flow. The most significant conclusions might be stated as:

1. As the magnetic parameter of the induced magnetic field increases, velocity exhibits both growing and decreasing behavior.

2. Increases in the reciprocal of the magnetic Prandtl number leads to larger horizontal components of the magnetic field.

3. The neural network method has created three models describing velocity, temperature, and concentration profiles.

When applied to the fluid flow problem at the electrical boundary layer, the Levenberg–Marquardt method and computational scheme prove to be a potent and flexible instrument. They are useful for designing and optimizing systems using electrical boundary layer fluid flow because they can be used to anticipate the flow and temperature distribution under various scenarios. The methodology mentioned above can be employed in developing and enhancing devices encompassing electrical boundary layer fluid flow, such as heat exchangers and power generators.

Author Contributions: Conceptualization, methodology, and analysis, M.S.A.; funding acquisition, A.S.B.; investigation, M.S.A.; methodology, M.S.A.; project administration, A.S.B.; resources, K.A.; supervision, K.A.; visualization, M.S.A.; writing—review and editing, M.S.A.; proofreading and editing, A.S.B. All authors have read and agreed to the published version of the manuscript.

Funding: This work was supported and funded by the Deanship of Scientific Research at Imam Mohammad Ibn Saud Islamic University (IMSIU) (grant number IMSIU-RG23014).

Data Availability Statement: The manuscript includes all required data and implementing information.

Acknowledgments: This research was supported by the Deanship of Scientific Research, Imam Mohammad Ibn Saud Islamic University (IMSIU), Saudi Arabia, Grant No. (IMSIU-RG23014).

Conflicts of Interest: The authors declare no conflict of interest to report regarding the present study.

Nomenclature

u	Horizontal component of velocity	μ_e	Magnetic permeability
v	Vertical component of velocity	ρ	Density of the fluid
T	Temperature of the fluid	σ	Electrical conductivity
C	Concentration	D_B	Brownian motion coefficient
H_x	IMF's component in the x -direction	D_T	Thermophoresis coefficient
H_y	IMF's component in the y -direction	c_p	Specific heat capacity
k_1	reaction rate parameter	T_w	Wall temperature
T_∞	Ambient temperature	C_w	Concentration at wall/sheet
C_∞	Ambient concentration	$\alpha_1 = \frac{1}{4\pi\rho}$	Magnetic diffusivity of the fluid
β, M	Magnetic parameters	δ	Reciprocal of the magnetic Prandtl number
E_c	Eckert number	N_b	Brownian motion parameter
P_r	Prandtl number	N_t	Thermophoresis parameter
S_c	Schmidt number	E_1	Local electric parameter
γ	Dimensionless reaction rate parameter		

References

- Iqbal, M.S.; Malik, F.; Mustafa, I.; Khan, I.; Ghaffari, A.; Riaz, A.; Nisar, K. Impact of induced magnetic field on thermal enhancement in gravity driven Fe_3O_4 ferrofluid flow through vertical non-isothermal surface. *Results Phys.* **2020**, *19*, 103472. [[CrossRef](#)]
- Kumar, D. Radiation effect on magnetohydrodynamic flow with induced magnetic field and Newtonian heating/cooling: An analytic approach. *Propuls. Power Res.* **2021**, *10*, 303–313. [[CrossRef](#)]
- Nawaz, Y.; Arif, M.S. Modified class of explicit and enhanced stability region schemes: Application to mixed convection flow in a square cavity with a convective wall. *Int. J. Numer. Methods Fluids* **2021**, *93*, 1759–1787. [[CrossRef](#)]
- Hayat, T.; Rashid, M.; Khan, M.I.; Alsaedi, A. Melting heat transfer and induced magnetic field effects on flow of water based nanofluid over a rotating disk with variable thickness. *Results Phys.* **2018**, *9*, 1618–1630. [[CrossRef](#)]
- Nawaz, Y.; Arif, M.S.; Shatanawi, W.; Nazeer, A. An explicit fourth-order compact numerical scheme for heat transfer of boundary layer flow. *Energies* **2021**, *14*, 3396. [[CrossRef](#)]
- Khan, S.A.; Hayat, T.; Alsaedi, A. Entropy generation in chemically reactive flow of Reiner-Rivlin liquid conveying tiny particles considering thermal radiation. *Alex. Eng. J.* **2023**, *66*, 257–268. [[CrossRef](#)]

7. Nawaz, Y.; Arif, M.S.; Bibi, M.; Abbasi, J.N.; Javed, U.; Nazeer, A. A Finite Difference Method and Effective Modification of Gradient Descent Optimization Algorithm for MHD Fluid Flow Over a Linearly Stretching Surface. *Comput. Mater. Contin.* **2020**, *62*, 657–677. [[CrossRef](#)]
8. Alsaedi, A.; Muhammad, K.; Hayat, T. Numerical study of MHD hybrid nanofluid flow between two coaxial cylinders. *Alex. Eng. J.* **2022**, *61*, 8355–8362. [[CrossRef](#)]
9. Muhammad, K.H.; Hayat, T.; Momani, S.; Asghar, S. FDM analysis for squeezed flow of hybrid nanofluid in presence of Cattaneo-Christov (C-C) heat flux and convective boundary condition. *Alex. Eng. J.* **2022**, *61*, 4719–4727. [[CrossRef](#)]
10. Chu, Y.-M.; Al-Khaled, K.; Khan, N.; Khan, M.I.; Khan, S.U.; Hashmi, M.S.; Iqbal, M.A.; Tlili, I. Study of Buongiorno's nanofluid model for flow due to stretching disks in presence of gyrotactic microorganisms. *Ain Shams Eng. J.* **2021**, *12*, 3975–3985. [[CrossRef](#)]
11. Alblawi, A.; Malik, M.Y.; Nadeem, S.; Abbas, N. Buongiorno's Nanofluid Model over a Curved Exponentially Stretching Surface. *Processes* **2019**, *7*, 665. [[CrossRef](#)]
12. Khatun, S.; Nasrin, R. Numerical Modeling of Buongiorno's Nanofluid on Free Convection: Thermophoresis and Brownian Effects. *J. Nav. Archit. Mar. Eng.* **2021**, *18*, 217–239. [[CrossRef](#)]
13. Akram, S.; Athar, M.; Saeed, K.; Razia, A.; Muhammad, T.; Hussain, A. Hybrid double-diffusivity convection and induced magnetic field effects on peristaltic waves of Oldroyd 4-constant nanofluids in non-uniform channel. *Alex. Eng. J.* **2023**, *65*, 785–796. [[CrossRef](#)]
14. Hasibi, A.; Gholami, A.; Asadi, Z.; Ganji, D.D. Importance of induced magnetic field and exponential heat source on convective flow of Casson fluid in a micro-channel via AGM. *Theor. Appl. Mech. Lett.* **2022**, *12*, 100342. [[CrossRef](#)]
15. Sakiadis, B.C. Boundary-layer behavior on continuous solid surfaces: I. Boundary-layer equations for two-dimensional and axisymmetric flow. *AIChE J.* **1961**, *7*, 26–28. [[CrossRef](#)]
16. Sakiadis, B.C. Boundary-layer behavior on continuous solid surfaces: II. The boundary layer on a continuous flat surface. *AiChE J.* **1961**, *7*, 221–225. [[CrossRef](#)]
17. Crane, L.J. Flow past a stretching plate. *Z. Angew. Math. Und Phys. ZAMP* **1970**, *21*, 645–647. [[CrossRef](#)]
18. Tsou, F.K.; Sparrow, E.M.; Goldstein, R.J. Flow and heat transfer in the boundary layer on a continuous moving surface. *Int. J. Heat Mass Transf.* **1967**, *10*, 219–235. [[CrossRef](#)]
19. Sadeghi, M.S.; Dogonchi, A.S.; Ghodrati, M.; Chamkha, A.J.; Alhumade, H.; Karimi, N. Natural convection of CuO-water nanofluid in a conventional oil/water separator cavity: Application to combined-cycle power plants. *J. Taiwan Inst. Chem. Eng.* **2021**, *124*, 307–319. [[CrossRef](#)]
20. Dogonchi, A.S.; Mishra, S.R.; Karimi, N.; Chamkha, A.J.; Alhumade, H. Interaction of fusion temperature on the magnetic free convection of nano-encapsulated phase change materials within two rectangular fins-equipped porous enclosure. *J. Taiwan Inst. Chem. Eng.* **2021**, *124*, 327–340. [[CrossRef](#)]
21. Sadeghi, M.S.; Tayebi, T.; Dogonchi, A.S.; Armaghani, T.; Talebizadehsardari, P. Analysis of hydrothermal characteristics of magnetic Al₂O₃-H₂O nanofluid within a novel wavy enclosure during natural convection process considering internal heat generation. *Math. Methods Appl. Sci.* **2020**. [[CrossRef](#)]
22. Abbasi, B.A.; Iqbal, J.; Ahmad, R.; Bibi, S.; Mahmood, T.; Kanwal, S.; Bashir, S.; Gul, F.; Hameed, S. Potential phytochemicals in the prevention and treatment of esophagus cancer: A green therapeutic approach. *Pharmacol. Rep.* **2019**, *71*, 644–652. [[CrossRef](#)] [[PubMed](#)]
23. Kudenatti, R.B.; Jyothi, B. Two-dimensional boundary-layer flow and heat transfer over a wedge: Numerical and asymptotic solutions. *Therm. Sci. Eng. Prog.* **2019**, *11*, 66–73. [[CrossRef](#)]
24. Basha, H.; Kumar, N.N.; Reddy, G.J. Effect of Prandtl number on leading edge accretion and ablation: A numerical study of unsteady boundary layer flow over a flat plate. *Heat Transf.—Asian Res.* **2019**, *48*, 2844–2881. [[CrossRef](#)]
25. Cortell, R. Flow and heat transfer of a fluid through a porous medium over a stretching surface with internal heat generation/absorption and suction/blowing. *Fluid Dyn. Res.* **2005**, *37*, 231–245. [[CrossRef](#)]
26. Dessie, H.; Kishan, N. MHD effects on heat transfer over stretching sheet embedded in porous medium with variable viscosity, viscous dissipation and heat source/sink. *Ain Shams Eng. J.* **2014**, *5*, 967–977. [[CrossRef](#)]
27. Abel, M.S.; Nandeppanavar, M.M.; Malkhed, M.B. Hydromagnetic boundary layer flow and heat transfer in viscoelastic fluid over a continuously moving permeable stretching surface with nonuniform heat source/sink embedded in fluid-saturated porous medium. *Chem. Eng. Commun.* **2010**, *197*, 633–655. [[CrossRef](#)]
28. Krishna, M.V.; Chamkha, A.J. Hall and ion slip effects on Unsteady MHD Convective Rotating flow of Nanofluids—Application in Biomedical Engineering. *J. Egypt. Math. Soc.* **2020**, *28*, 1. [[CrossRef](#)]
29. Krishna, M.V.; Chamkha, A.J. Hall effects on MHD squeezing flow of a water-based nanofluid between two parallel disks. *J. Porous Media* **2019**, *22*, 209–223. [[CrossRef](#)]
30. Krishna, M.V.; Swarnalathamma, B.V.; Chamkha, A.J. Investigations of Soret, Joule and Hall effects on MHD rotating mixed convective flow past an infinite vertical porous plate. *J. Ocean. Eng. Sci.* **2019**, *4*, 263–275. [[CrossRef](#)]
31. Krishna, M.V.; Ahammad, N.A.; Chamkha, A.J. Radiative MHD flow of Casson hybrid nanofluid over an infinite exponentially accelerated vertical porous surface. *Case Stud. Therm. Eng.* **2021**, *27*, 101229. [[CrossRef](#)]
32. Damseh, R.A.; Al-Odat, M.Q.; Chamkha, A.J.; Shannak, B.A. Combined effect of heat generation or absorption and first-order chemical reaction on micropolar fluid flows over a uniformly stretched permeable surface. *Int. J. Therm. Sci.* **2009**, *48*, 1658–1663. [[CrossRef](#)]

33. Chamkha, A.J.; Khaled, A.R.A. Similarity solutions for hydromagnetic simultaneous heat and mass transfer by natural convection from an inclined plate with internal heat generation or absorption. *Heat Mass Transf.* **2001**, *37*, 117–123. [[CrossRef](#)]
34. Javadpour, R.; Heris, S.Z.; Mohammadfam, Y.; Mousavi, S.B. Optimizing the heat transfer characteristics of MWCNTs and TiO₂ water-based nanofluids through a novel designed pilot-scale setup. *Sci. Rep.* **2022**, *12*, 15154. [[CrossRef](#)] [[PubMed](#)]
35. Sarvari, A.A.; Heris, S.Z.; Mohammadpourfard, M.; Mousavi, S.B.; Estellé, P. Numerical investigation of TiO₂ and MWCNTs turbine meter oil nanofluids: Flow and hydrodynamic properties. *Fuel* **2022**, *320*, 123943. [[CrossRef](#)]
36. Karimi Shoar, Z.; Pourpasha, H.; Zeinali Heris, S.; Mousavi, S.B.; Mohammadpourfard, M. The effect of heat transfer characteristics of macromolecule fouling on heat exchanger surface: A dynamic simulation study. *Can. J. Chem. Eng.* **2023**, *101*, 5802–5817. [[CrossRef](#)]
37. Rahmanzadeh, M.; Asadi, T.; Atashafrooz, M. The Development and Application of the RCW Method for the Solution of the Blasius Problem. *J. Appl. Comput. Mech.* **2020**, *6*, 105–111.
38. Atashafrooz, M.; Sajjadi, H.; Delouei, A.A. Interacting influences of Lorentz force and bleeding on the hydrothermal behaviors of nanofluid flow in a trapezoidal recess with the second law of thermodynamics analysis. *Int. Commun. Heat Mass Transf.* **2020**, *110*, 104411. [[CrossRef](#)]
39. Rehman, K.U.; Shatanawi, W.; Asghar, Z.; Bahaidarah, H.M.S. Neural networking analysis for MHD mixed convection Casson flow past a multiple surfaces: A numerical solution. *AIMS Math.* **2023**, *8*, 15805–15823. [[CrossRef](#)]
40. Zhao, J.; Nguyen, H.; Nguyen-Thoi, T.; Asteris, P.G.; Zhou, J. Improved Levenberg-Marquardt backpropagation neural network by particle swarm and whale optimization algorithms to predict the deflection of RC beams. *Eng. Comput.* **2022**, *38*, 3847–3869. [[CrossRef](#)]
41. Nguyen, H.X.; Cao, H.Q.; Nguyen, T.T.; Tran, T.N.C.; Tran, H.N.; Jeon, J.W. Improving robot precision positioning using a neural network based on Levenberg Marquardt–APSO algorithm. *IEEE Access* **2021**, *9*, 75415–75425. [[CrossRef](#)]
42. Ali, M.S.; Ayaz, M.; Mansoor, T. Prediction of discharge through a sharp-crested triangular weir using ANN model trained with Levenberg-Marquardt algorithm, model. *Earth Syst. Environ.* **2022**, *8*, 1405–1417. [[CrossRef](#)]
43. Ye, Z.; Kim, M.K. Predicting electricity consumption in a building using an optimized backpropagation and Levenberg-Marquardt backpropagation neural network: Case study of a shopping mall in China. *Sustain. Cities Soc.* **2018**, *42*, 176–183. [[CrossRef](#)]
44. Rehman, K.U.; Shatanawi, W.; Çolak, A.B. Levenberg–Marquardt Training Technique Analysis of Thermally Radiative and Chemically Reactive Stagnation Point Flow of Non-Newtonian Fluid with Temperature Dependent Thermal Conductivity. *Mathematics* **2023**, *11*, 753. [[CrossRef](#)]
45. Al Salman, H.J.; Nawaz, Y.; Al Ghafli, A.A. An Implicit Finite Difference Scheme and Neural Network Approach for Non-Newtonian Nanofluid Flow Using Induced Magnetic Field. *Mathematics* **2023**, *11*, 2089. [[CrossRef](#)]
46. Hayat, T.; Mustafa, M.; Pop, I. Heat and mass transfer for Soret and Dufour’s effect on mixed convection boundary layer flow over a stretching vertical surface in a porous medium filled with a viscoelastic fluid. *Commun. Nonlinear Sci. Numer. Simul.* **2010**, *15*, 1183–1196. [[CrossRef](#)]
47. Yih, K.A. Free convection effect on MHD coupled heat and mass transfer of a moving permeable vertical surface. *Int. Commun. Heat Mass Transf.* **1999**, *26*, 95–104. [[CrossRef](#)]

Disclaimer/Publisher’s Note: The statements, opinions and data contained in all publications are solely those of the individual author(s) and contributor(s) and not of MDPI and/or the editor(s). MDPI and/or the editor(s) disclaim responsibility for any injury to people or property resulting from any ideas, methods, instructions or products referred to in the content.